Strata structure interpretation and mud volcanism activity analysis at the Zhurong landing site

Xiaojian Xu[1,2,3], Zhizhong Kang[1,2,3*], Yu Yang[1,2,3], Teng Hu[1,2,3], Dong Wang[4] Xing Du[1,2,3], Juan Xie[1,2,3], Yehua Ma[1,2,3]

[1]School of Land Science and Technology, China University of Geosciences (Beijing), Beijing, China; [2]Research Center of Lunar and Planetary Remote Sensing Exploration, China University of Geosciences (Beijing), Beijing, China; [3]Subcenter of International Cooperation and Research on Lunar and Planetary Exploration, Center of Space Exploration, Ministry of Education of the People's Republic of China, Beijing, China; [4]Changchun Institute of Optics, Fine Mechanics and Physics, Chinese Academy of Sciences, Changchun, China

Abstract

China's first Mars Exploration Mission Tianwen-1 achieved full success. The loaded Zhurong Rover landed south of the Utopia Planita. The Tianwen-1 orbiter also sending back high-resolution images. We utilized the High-Resolution Imaging Camera (HiRIC) of Tianwen-1 and Context Camera loaded on the Mars Reconnaissance Orbiter to collect the image data and construct a 3D strata model of the Zhurong landing site. Using this model, we analyzed the material loss of ghost craters. Judging from the morphological characteristics of pitted cones at the Zhurong landing site, we confirmed their classification as mud volcanoes. We also analyzed the possible cause of formation by combining the gravity field and magnetic field data. The experimental results indicate that (1) the Zhurong landing site can be divided into the dry sedimentary, moisture sedimentary, and Vastitas boreal (VB) members as three strata and another ejecta blocks. The three strata are categorized into VB formations with an integral width of 1.2 km. (2) The cones at the Zhurong landing site are mud volcanoes formed by groundwater thermal activity, and the heat source originate from a southern underground magma chamber. The density of mud volcanoes signifies the existence of ejecta blocks. (3) Apart from volumetric compaction, some ghost craters show eruption of underground substances. Generally, after the VB unit located on the surface of the Zhurong landing site surface formed 3.43Ga, the current geomorphology of the landing site was altered due to interior and exterior geological activities, such as the differentiation of water evaporation above ground and underground, underground thermal activity, and meteorite impacts.

Plain Language Summary

The water environment and its evolution history on Mars is one of the important research topics of planetary science. Tianwen-1 Mission and Zhurong Rover landed in the south of Utopia Planita and provides the latest data for the investigation on this topic. By taking advantage of these high-resolution

images combined with collected data from past Mars Exploration Missions, we constructed a 3D strata model at the Zhurong landing site to confirm the three-layered structure and ejecta blocks at the site. Through morphological analysis, we determined that the cones at the site are very likely mud volcanoes and discovered the thermal power source formed by combining gravity fields and magnetic data. Our research shows that the Zhurong landing site covers paleomarine sediments 1.2 km wide. After the disappearance of surface water at the site approximately 3.43 bn years ago, effects including water evaporation differences above ground and underground, underground thermal activity and meteorite collision characterize the formation of geographical morphology at the site.

Key points

- 3D strata model suggests that volume compaction coincides with underground material ejection during the formation of partial ghost craters.
- The cones at Zhurong landing site are mud volcanoes, the underground magma chamber in the south is the heat source for their formation.
- After VBF formed at 3.43Ga, water evaporation, underground thermal activity and meteorite impacts cause the lanform at Zhurong landing site.

1. Introduction

Zhurong Rover, China's first Mars rover equipped with the Tianwen-1 (TW-1) lander, successfully landed at the target site in southern Utopia Planita on 15th May 2021. TW-1 Mission plans to achieve orbiting, landing and roving on Mars to carry out globally and synthetically orbital survey and regionally patrol exploration in a launch. Thus, the TW-1 detector consists of an orbiter and lander, and the lander contains an entry capsule and rover. There are five scientific objectives in the TW-1 Mission: (1) Mars morphology and geological structure characteristics; (2) Soil characteristics and water/ice distribution on the surface; (3) Material composition on the surface; (4) Atmospheric ionosphere, surface climate and environmental characteristics; and (5) Physical field and internal structure. Based on these objectives, southern Utopia Planita was chosen as the landing site. At present, the Zhurong Rover is traveling to the ancient coast to the south to implement the expansion task. Investigation by the Zhurong Rover and TW-1 orbiter can help researchers study the evolution of the paleo-ocean environment and the features of water/ice activities in the southern Utopia Planita.

Through the statistical analysis of 10–55° N, 210–260° W cones in the Utopia Planita, Depablo et al. (2009) believes that the formation of cones in this area is related to mega lahars, debris flows and outflows in Elysium Province and the Utopia Planita. Soare et al. (2005, 2013, 2020) conducted continuous research that lasted over a decade. The morphologies, scale, height and surface textures

of the cones on the Utopia Planita are consistent with Tuktoyaktuk Coastlands in northern Canada, closed-system ice core pingos in north central Alaska and northeast Russia on Earth. Therefore, the cones on the Utopia Planita are not only evidence showing the former existence of liquid water on the Mars surface but also marks of freeze–thaw cycling of the Amazonian ice layer. Ivanov et al. (2014) utilized high-resolution images covering approximately 80-85% of the selected region in the Utopia Planita to conduct detailed mapping and discover the mud volcanism landforms represented by etched flows. Therefore, it is considered that there are a large number of water bodies in the middle of the Utopia Planita. Recently, Mangold et al. (2021) employed the returned data of the perseverance rover and the presence of strata discovered at the western edge of Jezero crater by HiRSE imaging. They further analyzed and discovered that intermittent floods occurred in the region, and explored ancient lakes that may have transitioned from sustained hydrologic activity in a persistent lake environment to highly energetic short-duration fluvial flows. For Tianwen-1's landing site, Wu et al. (2021) utilized multiple sourced MRO data and the Mars Global Surveyor (MGS) to conduct a geographical investigation of the thermophysical properties, landform features, and substance compositions of the region to highlight what the Tianwen-1 Mission has determined as critical information for the study of water environment evolution in the region. It is noteworthy that the current research results mainly involve the interpretation of surface morphology. If the spatial structure distribution of strata can be further interpreted by remote sensing technology, it will contribute to the interpretation of the regional geological evolution history.

Currently, the interpretation of stratigraphic structure has made some progress in the study of lunar surface stratigraphy. Long et al. rely on Lunar Penetrating Radar's probing result and regional geology of the Change-3 landing site to comprehensively determine and explain the 9 subsurface layer positioning (Long, 2015). Yuan et al. adopted the 9 startified strata by Long et al. to explain the sequence of lava flow sedimented on the lunar surface at different periods. They inferred the direction of these flows from the perspective of layer depth, width and other geological information. The explained section imaging results show that the landing points of Change-3 and Apollo have similar underground structures (Yuan, 2017). Yue et al. estimated the thickness of the weathered layer of the Change-5 landing site by measuring concentric craters. The results indicate that the regolith range of the site is 0.74~18.00 m (Yue, 2019). Fa et al. acquired the thickness upper and lower limits of the weathered layer via concentric and normal craters. Their results show that 50% of the thickness of the weathered layer in Sinus Iridum ranges from 5.1~10.7 m, the average and median weathered layer thicknesses vary from 8.5~8.0 m, and there is a distinctive site difference in the weathered layer width. The middle value of the majority of sites vary from 2.6~12.0 m. Therefore, relying on remote sensing data to interpret strata is the key for stratified layer interpretation.

This paper measures the depth of flat-bottomed craters via high-resolution image production technology to construct a 3D strata model of the Zhurong landing

site and accomplish the interpretation of strata. By analyzing and estimating the water ice layer buried depth in the crater, the team determined the spatial distribution of the water-containing ice layer. The team further utilized multiple source data of gravity and magnetic fields to interpret the strata structure in the landing site to explore the mud volcano formation reason and scale at the Zhurong landing site to facilitate water thermal activity and evolutionary history studies at the Zhurong landing site.

2. Study Area and Data

2.1 Study Area

At 7:18 on May 15, 2021, the Tianwen-1 Landing Patrol - Zhurong Rover completed a successful landing. The landing site located at 109.92°E, 25.06°S is the junction of ancient land and ocean at the southern end of the Utopia Planita in the Northern Hemisphere of Mars.

Utopia Planita is the largest plane on Mars with a diameter of 3200 km. Its center is located at 49.7°N, 118°E and was formed during the Noachian (McGill, 1989). The southern region of the Utopian Planita is flat with a lack of large meteorite craters or gullies. The terrain around the Utopian basin is complex. The edge of the basin is the crustal dichotomy boundary in the south and west of Mars, the southwest is adjacent to Isidis Planita, the east is adjacent to Elysium Province, and an unnamed arcuate ridge acts as the dividing line between the north polar and the Utopian basin (Thomson, 2001). The geomorphic characteristics of the Utopia Planita show that this area may be an ancient ocean, which is closely related to the evolution of the Martian water environment, making it an important area in Martian exploration (Ivanov, 2014). In addition to the Mars Rover Zhurong, American Viking 2 Mars probe and the Perseverance Rover also landed and conducted exploration missions in the Utopian Planita in September 1976 and February 2021, respectively (Masursky, 1976; Mangold, 2021). There are many special geomorphic units in the southern Utopian Planita, such as rampart craters, pancake-like ejecta craters, ghost craters, mesas, dunes, etc. (Mills, 2021). These special geomorphic structures show that the region once had water ice and experienced more intense volcanic activity and wind sand erosion. This area contains a substance called Vastitas Borealis, abbreviated as VB. The VB is a Late Hesperian geomorphic unit, covering most of the northern lowlands of Mars (Tanaka, 1987). Kreslavsky et al. (Kreslavsky, 2002) believe that this material is composed of marine sediments formed by floods released from outflow channels. The possibility of such an ocean is important because it is related to the potential habitability of ancient Mars.

2.2 Data

All the data in the paper include CTX mosaic images (5 m/pixel resolution, Dickson, 2018) produced by the Malin Space Science Systems and Jet Propulsion Laboratory and panchromatic images (0.7 m/pixel) of the Tianwen-1 high-

resolution camera (HiRIC); HiRIC is one of the main payloads of China's first Mars Exploration Mission. Its main goal is to obtain detailed observation images of key areas on the surface of Mars. It has two working modes: panchromatic mode and multispectral mode (Meng, 2021). The comparison of key parameters between HiRIC and MRO equipped with HiRISE and CTX is shown in Table 1 (Meng, 2021; McEwen, 2007; Malin, 2007). Both HiRIC and HiRISE can provide high-resolution images to characterize the strata, geological structure and composition of Martian surface features in detail (McEwen, 2007); CTX is designed to provide background data obtained by other instruments (Malin, 2007). After comprehensively evaluating the performance parameters and research area of the above three instruments, we selected HiRIC panchromatic images and CTX images. The high-resolution images and DEM offered by HiRIC provide clear morphological features of large areas in the southern Utopia Planita, which can also accomplish mud volcano statistics and land block division that could not be completed originally due to the small coverage area of HiRISE (Figure 1). 1 (a), red is the coverage area of the HiRIC image, yellow is the coverage area of the HiRISE image) and insufficient CTX resolution (Figure. 1 (Bb c)) It has provided great help for the regional research.

HiRIC DEM (3.5 m/pixel), CTX DEM (6 m/pixel) and MEX HRSC MOLA blended DEM (200 m/pixel, Ferguson, 2018) produced by stereophotogrammetry. The HiRIC DEM is used for stratigraphic surveys and block division, the CTX DEM is used for stratigraphic surveys, and the MEX HRSC MOLA blended DEM is used for the analysis of large-scale geomorphic units.

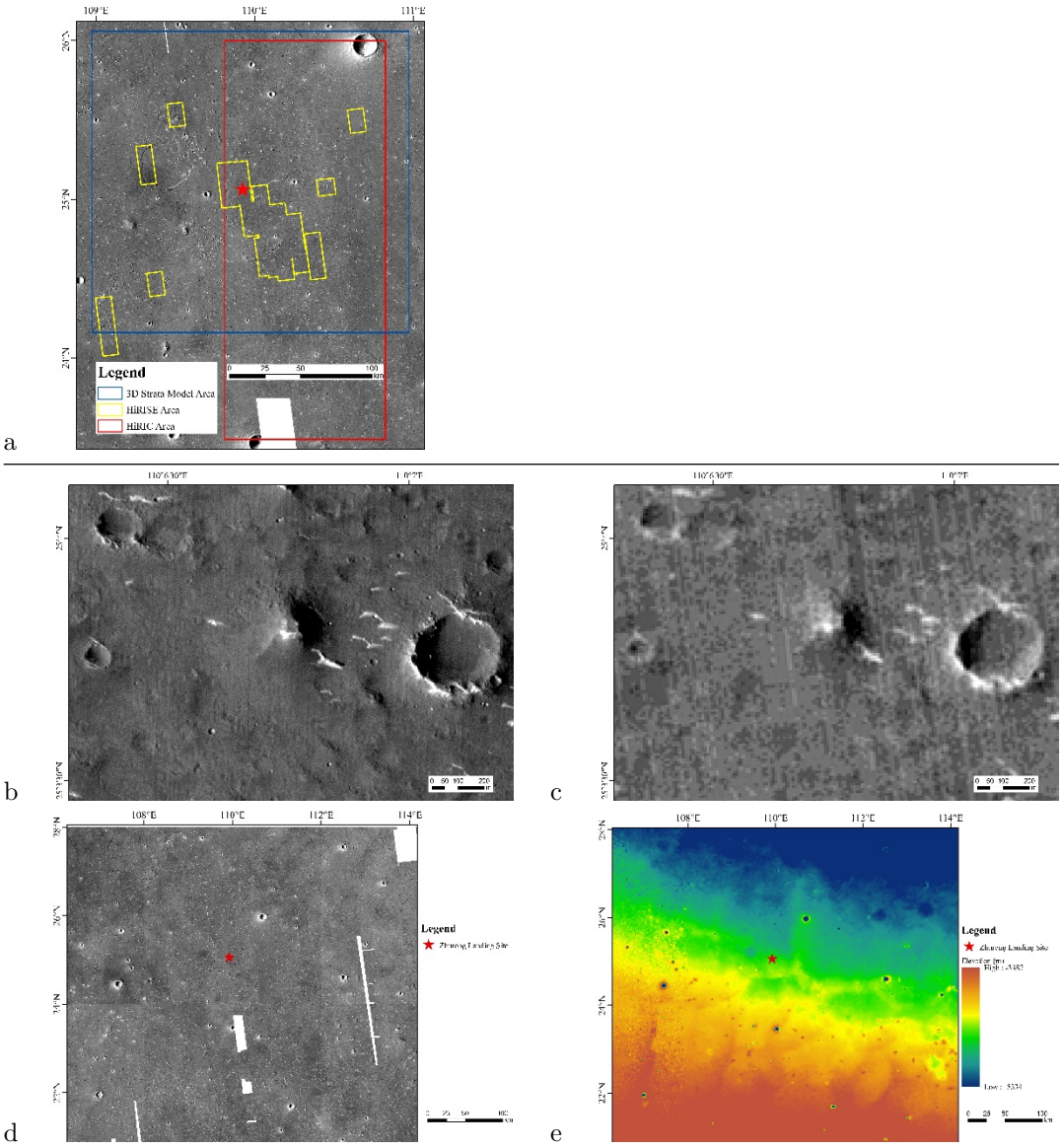
a
109°E
110°E
111°E
26°N
25°N
24°N
Legend
3D Strata Model Area
HiRISE Area
HiRIC Area
0 25 50 100 km
b
110°6'30"E
1.0°2'E
25°N
0 50 100 200 m
c
110°6'30"E
1.0°2'E
25°N
0 50 100 200 m
d
108°E
110°E
112°E
114°E
28°N
26°N
24°N
22°N
Legend
e
108°E
110°E
112°E
114°E
26°N
25°N
24°N
Legend
0 25 50 100 km

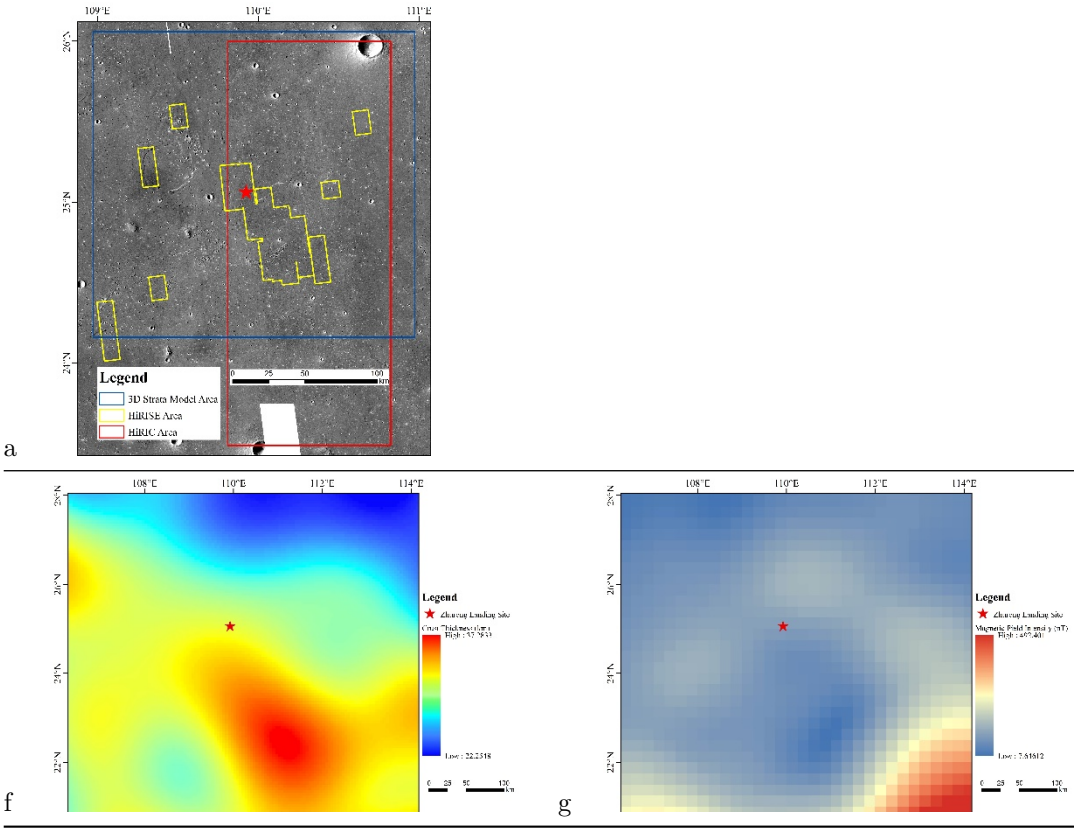

Figure 1 (a) Blue: 3D strata model range, red: HiRIC image coverage, yellow: HiRISE coverage (CTX mosaic ID: E108_N20, E108_N24); (b) Mud volcano on HiRIC image; (c) Mud volcano on CTX image (CTX mosaic ID: E108_N24); (d) CTX images produced by Malin Space Science System and Jet Propulsion Laboratory in the landing site of Zhurong(CTX mosaic ID: E104_N20, E104_N24, E108_N20, E108_N24, E112_N20, E112_N24); (e) MEX HRSC MOLA Blended DEM in the landing site of Zhurong; (f) Crustal thickness map of Zhurong landing site; (g) Magnetic field intensity diagram of Zhurong landing site;.

Crustal thickness data (Goossens et al. (2017)). Goossens et al. (2017) calculated the Martian crust thickness based on the NASA GMM-3 gravity model and MOLA topography. A standard density value model of 2900 kg/m^3 is adopted for the crust, and 3500 kg/m^3 is adopted for the mantle.

Mars magnetic field model (160 km/pixel) (Langlais et al. (2019)). Langlais et al. (2019) used MGS magnetometer, electron reflectometer and MAVEN (Mars Atmosphere and Volatile Evolution) magnetometer data to reflect the magnetic field on a sphere with a radius of 3393.5 km. Gravity and magnetic field

observations are used to find possible traces of underground tectonic movement.

Table 1 Comparison of parameters among HiRIC CTX and HiRISE

Data	Design resolutions	Height of designed rail	Focal length	Aperture	Sideview	Wave segment	CCD dimension	CCD quantity
HiRIC	Panchromatic 0.5/pixel, Multispectral 2/pixel	km	m	f/12	°, 9 km	Panchromatic 450 nm 900 nm Multispectral 450 nm 520 nm, 520 nm 600 nm, 520 nm 600 nm, 760 nm 900 nm	μm	
CTX	m/pixel	km	mm	f/3.25	°, 30 km	~700 nm	μm	
HiRISE	m/pixel,	km	mm	f/24	Red 1.141°, 6 km Color 0.23°, 1.2 km	Red 570~830 nm Turquoise <580 nm Near infrared >790 nm	μm	Red 20048 Colored 4048

3. Method

The research roadmap of this paper is shown in Figure 2. First, the stratigraphic structure and surface ejecta distribution of the Zhurong landing site are obtained by using the CTX and HiRIC DEM combined with morphological methods. On this basis, the three-dimensional strata model and ejecta block distribution map are made. The three-dimensional strata model is used for the analysis of strata and ghost craters. Based on the distribution map of the ejecta block, combined with gravity and magnetic data, this paper analyzes the genesis of mud volcanoes and finally analyzes the regional geological evolution characteristics

and dynamic mechanism after the formation of the VB.

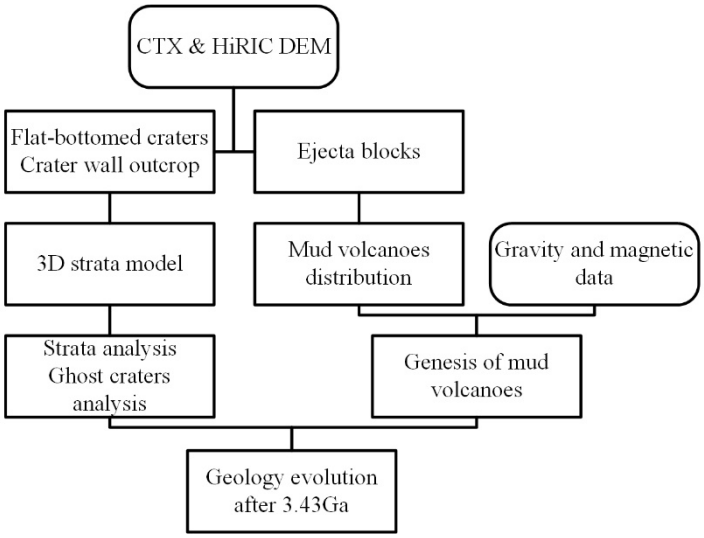

Figure 2 The process of experimental methods

3.1 Morphological method

The surface morphology of Mars is diverse. There are rampart craters (Figure. 3 (a)), pancake-lie ejecta craters (Figure. 3 (b)), ghost craters (Figure. 3 (c)), mesas (Figure. 3 (d)), dunes (Figure. 3 (E)), cones (Figure. 3 (f)) and so on in the south of Utopia Planita. These unique landforms are the yields of flowing water (Figure. 3 (a-c)), glacier (Figure. 3 (d)) or atmospheric action (Figure. 3 (e)), which can reflect the paleogeographic environment and evolution history. The special shape of craters can be used as evidence of stratigraphic correlation, assist in the construction of a three-dimensional strata model and indicate the spatial distribution of water bearing strata. Statistics of the spatial distribution characteristics of special landforms, combined with topographic changes, can quantitatively describe the regional characteristics for the division and evolution analysis of different plots.

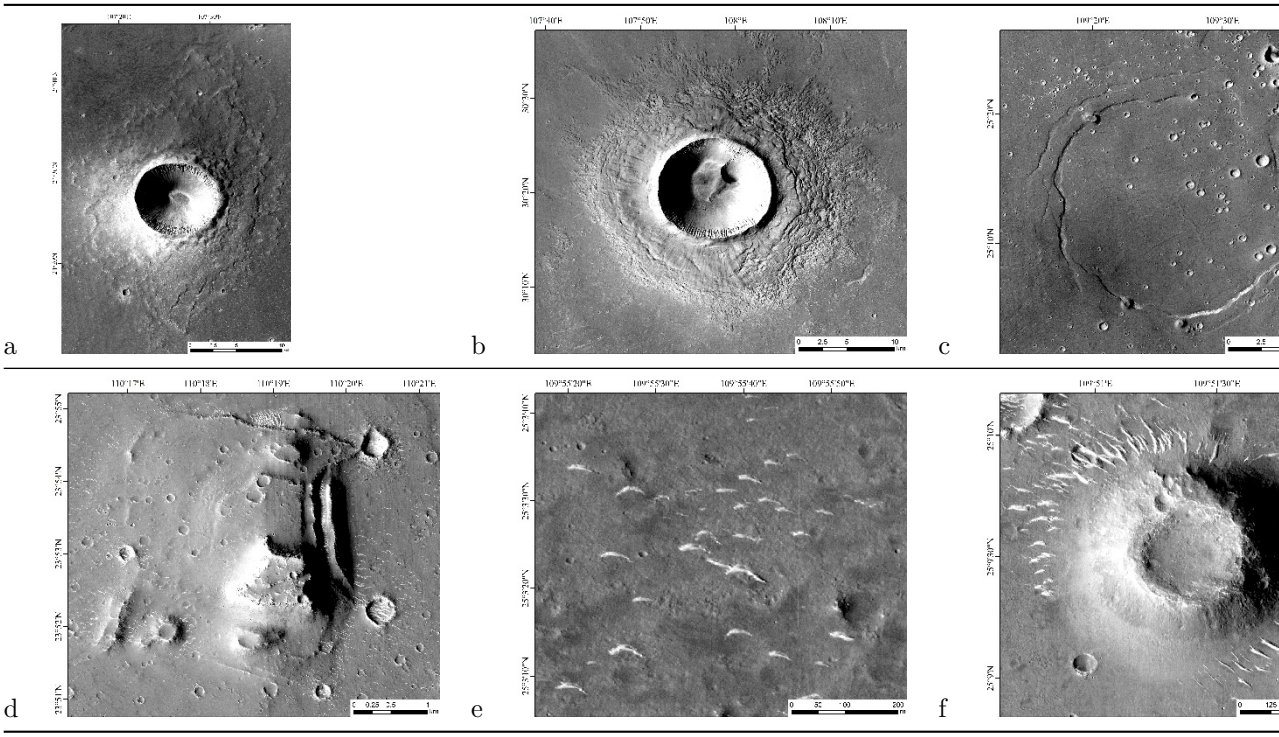

Figure 3 (a) Rampart crater(CTX mosaic ID: E104_N24), (b) pancake-like ejecta crater(CTX mosaic ID: E104_N28, E108_N28), (c) ghost crater(CTX mosaic ID: E108_N24), (d) mesas, (E) dune, (f) cone.

The rampart crater reflects the distribution of underground water ice (Barlow, 2006), and the burial depth of underground water ice can be estimated by measuring its depth (Niu, 2021). Ghost craters can also be used to study sediment thickness. Some ghost craters have two concentric circular grabens. The thickness of the filler can be estimated by measuring the diameter of rampart craters and the distance of concentric grabens (Mills, 2021). The genesis of the cone is still controversial, mainly including mud volcano, cinder and rootless cone hypotheses (Dapremont, 2021). Various hypotheses have specific genesis and formation environments. Determining the genesis of the cone through morphological characteristics can determine the geological environment of the Zhurong landing site during the formation of the cone.

3.2 Measurement of stratigraphic structure and generation of the 3D strata model

When the meteorite energy is high, it will penetrate one or more strata in the process of impact with the planet's surface, making the crater a natural outcrop. Due to the different compositions and mechanical properties of different strata,

the crater presents special forms, such as flat bottoms and concentric circles. Therefore, the stratum structure can be measured based on the morphological characteristics of the stratum exposed in the crater (Wilcox, 2005). In Figure. 4 (a), the depth of the exposed stratum can be obtained by measuring the flat bottom marked by the green ring through the DEM. In addition, each stratum exposed on the impact pit wall may also show different textures and material compositions. The stratum can be identified by high-resolution or spectral images (Figure. 4 (b)). The weathering of the planetary surface will lead to the degradation of the crater, making it difficult to identify the formation characteristics. The sand and dust on Mars will also fill the interior of the crater, and the strata thickness cannot be measured accurately (Figure 1). 4 (c)). Therefore, when measuring the formation depth, it is necessary to select a fresh impact pit to eliminate the error.

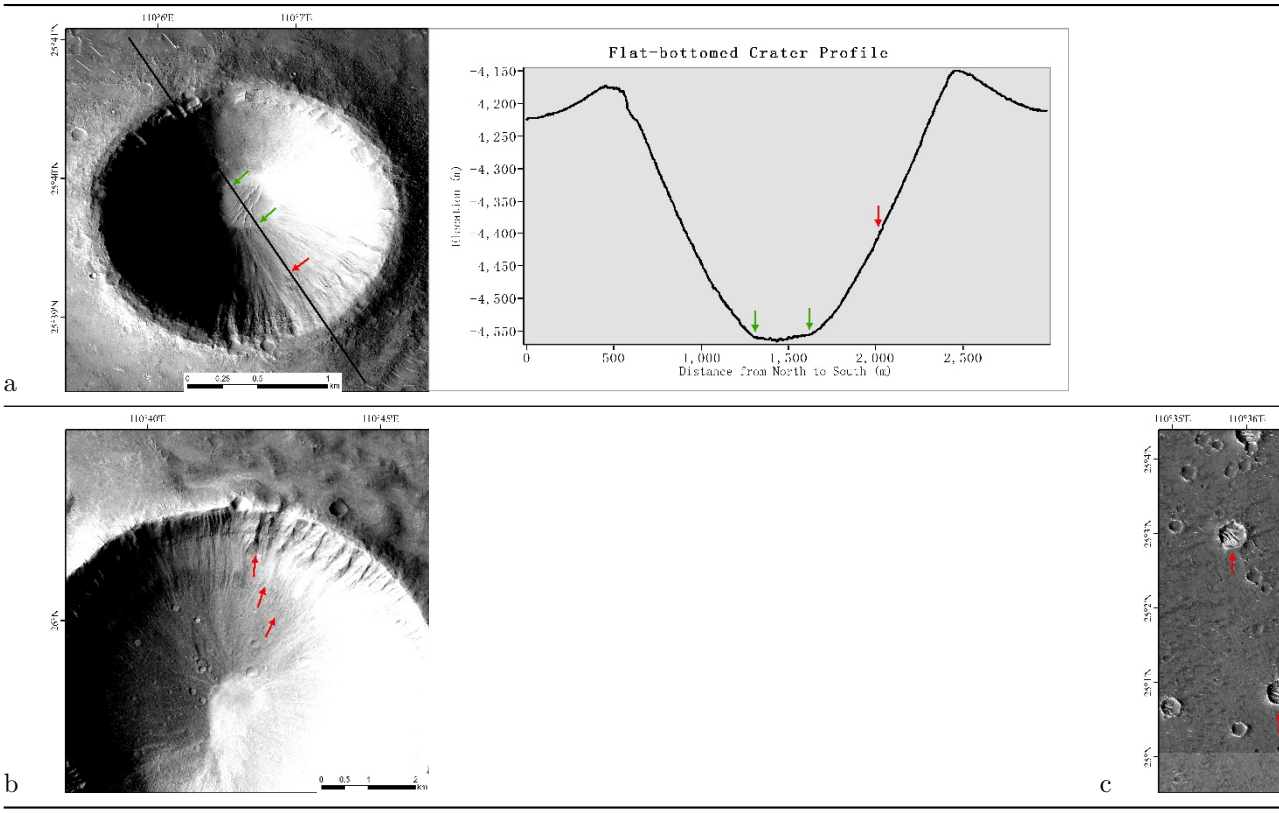

Figure 4 (a) Flat bottom crater and pit wall stratum outcrop; (b) Pit wall formation outcrop(CTX mosaic ID: E108_N24); (c) There are obvious dunes at the bottom of craters buried by aeolian sand.

We realized the stratigraphic interpretation of the Zhurong landing site by con-

structing a three-dimensional strata model. Accurate measurement of the formation structure requires a DEM with high accuracy. However, the resolution of the existing global DEM: MEX HRSC MOLA blended DEM is only 200 m, which cannot meet the needs of formation depth measurement. Hence, we used CTX image and stereo image matching to make the CTX DEM of the Zhurong landing site (Figure 1.5 (a)). However, due to the limitation of CTX image overlap, the final DEM will have missing data in many places. Therefore, when measuring the stratum, we only obtain the depth relative to the surface, rather than the absolute elevation overlap and use the HiRIC DEM to supplement the stratum measurement data where CTX DEM data are missing (Figure. 5 (b)).

The MEX HRSC MOLA blended DEM shows that the terrain of the Zhurong landing site is very flat, so it is feasible for us to use planes to simulate the surface of the Zhurong landing site and determine the depth of each stratum. Although DEM products provided by HiRIC (60 km $\times$ 150 km) cover only the eastern half of the three-dimensional stratum model, they still provide us with a method to test the reliability of stratum depth measurements. After comparison, we find that the difference between the formation depth measured by the CTX DEM and that measured by the HiRIC DEM is less than 10 m, which is less than 1% of the thickness of the VB group and has no impact on the formation interpretation results. It is shown that the method of measuring formation depth by a high-resolution DEM is reliable.

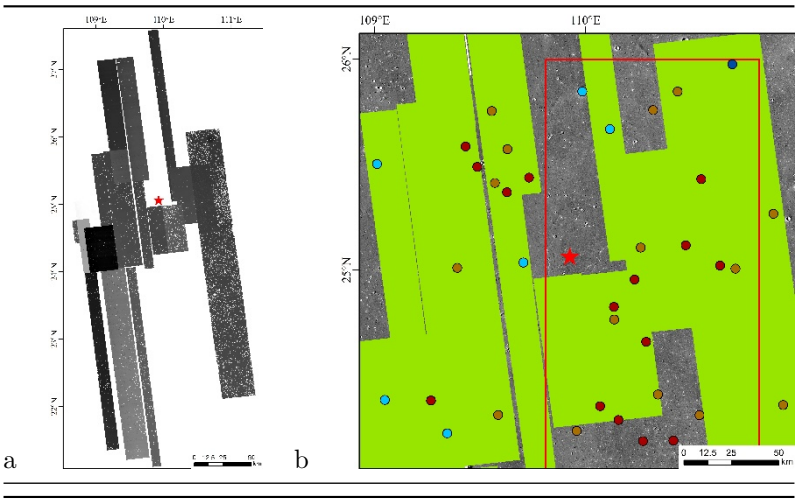

Figure 5 (a) DEM generated by CTX stereo relative, (b) comparison of high-resolution DEM coverage area, red: HiRIC DEM coverage, green: CTX stereo relative DEM coverage, point: crater for stratum measurement. Some craters are located outside the CTX DEM and measured by the HiRIC DEM.

When comparing strata, we comprehensively consider the statistical law, crater shape and regional tectonic background. According to the regional tectonic

background, there is no large-scale compression and tensile structure and no trace of magmatic erosion at the Zhurong landing site, so the strata in this area are distributed horizontally. The strata to which the measurement results belong are clustered by the shape of craters. The formation types include the following: (1) the corrugated sputter sheet cannot be formed, and a large amount of gravel (Figure. 6 (a) red arrow) or secondary crater (Figure. 6 (a) yellow arrow) are scattered around the fresh crater, and some large crater walls show the dry sedimentary rock section of this layer, which is rough (Figure 6 (a) green arrow); (2) The outside of the crater is corrugated (Figure. 6 (b)), and the wet sedimentary rock section with high water content; (3) The depth is significantly greater than most sections, with crater barriers (Figure 6. (c)), showing the VB section with more water/ice. In addition, there are no rocks or secondary craters around the impact craters, which may correspond to the ejecta block (Figure. 6 (d)).

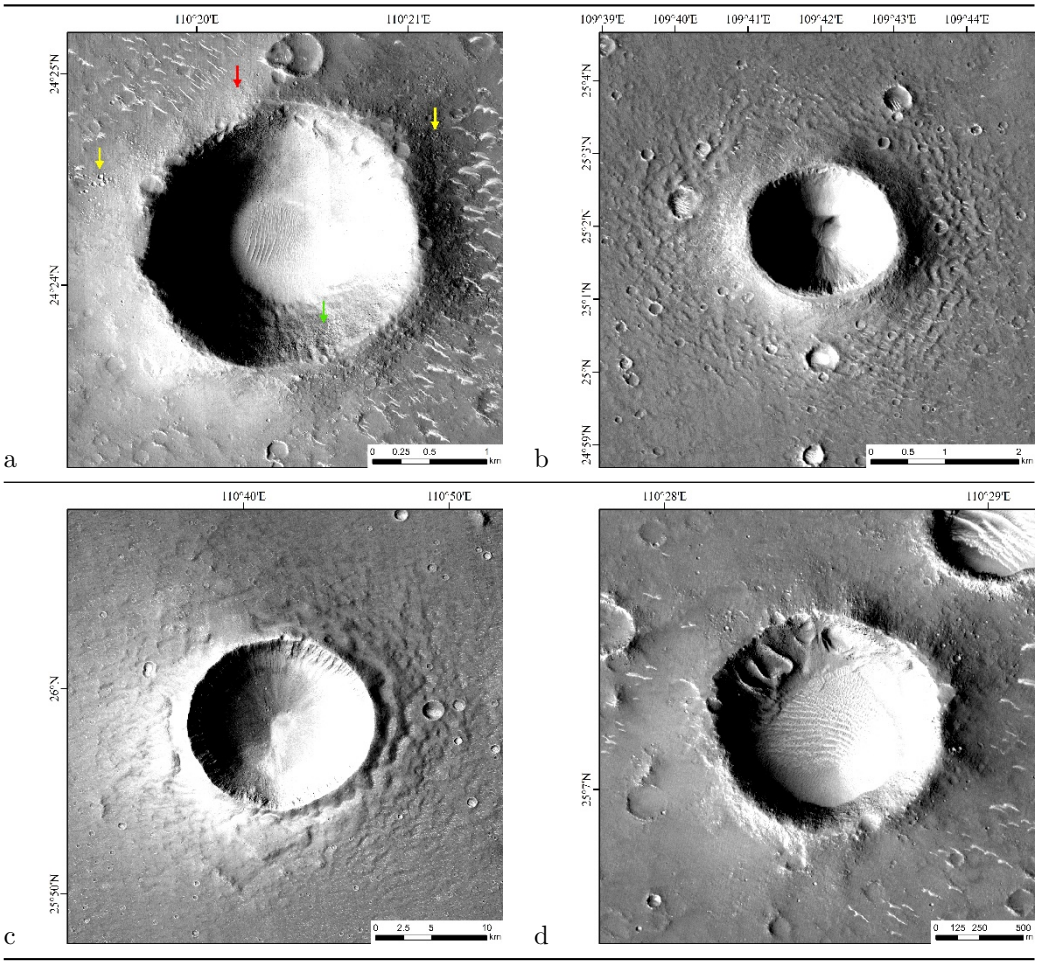

Figure 6 (a) Crater corresponding to the dry sedimentary rock section: dry outside the pit, with sputtered stones (red arrow), secondary craters (yellow arrow) and rough crater walls (green arrow); (b) Crater corresponding to the wet sedimentary rock section: the corrugated texture formed in the wet environment appears outside the crater (CTX mosaic ID: E108_N24); (c) Crater corresponding to the VB section: forming barrier(CTX mosaic ID: E108_N24); (d) Ejecta layer crater: the outside of the pit is dry with few stones and no secondary craters

3.3 Analysis of crustal thickness and magnetic field anomalies

The anomaly of the planetary gravity field is caused by the fluctuation of the surface shape of its star and the spatial anomaly distribution of the internal material density. The planetary crustal thickness can be retrieved by combining gravity data with topography. The crustal thickness reflects the transformation of the crustal layer by magmatic activity (Wieczorek, 2004). The thickness of the crust is affected by a variety of geological processes, such as meteorite impact and mantle uplift, which will lead to the thinning of the crust, while the crust will be thickened after the magma from volcanic eruption solidifies. The analysis of the distribution characteristics of crustal thickness can help to find the deep dynamic process causing the change in surface morphology. To more clearly find the abnormal changes of crustal thickness on the image, we use the "stretched" renderer to display the continuous crustal thickness in the color of smooth gradient of the full spectrum of the red to blue visible band, and use the percentage truncation method to estimate the maximum 5% and minimum 5% of the crustal thickness in the study area, and map to the red and blue end of the color band, respectively to enhance the contrast of the crustal thickness image.

In the study of the internal structure and formation of planets, the magnetic field is also one of the important physical fields to study planets. Martian remanence is closely related to the Martian geological structure and internal dynamic process. After the shutdown of the Martian generator, large-scale magmatic activity will cause the magnetic body to be heated and demagnetized, so the magnetic field intensity is low in the younger igneous rocks on Mars (Mittelholz, 2020). In addition, large-scale crater events damage the upper crust containing strongly magnetized materials, resulting in the weakening of magnetic field intensity in some areas (Gong, 2021). Due to the low resolution (0.25°/pixel) of the magnetic field intensity image on the surface of Mars, the isoline of the magnetic field intensity is extracted in the experiment to find the magnetic anomaly.

It is difficult to judge the origin of a single crustal thickness and magnetic anomaly. Therefore, combined with previous research results (Wieczorek, 2004; Mittelholz, 2020; Gong, 2021), we observe whether there is a magnetic field intensity anomaly at the location of the crustal thickness anomaly found and observe the following morphological characteristics: (1) the gravity and mag-

netic anomaly caused by the meteorite impact is judged by the area covered by a large crater with thin crust and weak magnetic field intensity; (2) if the crust is thickened and the area with a magnetic anomaly is covered by volcano or lava, it is recognized as volcanic activity; and (3) if the crust is thickened and there is a magnetic anomaly, and there are no obvious characteristics such as volcanic activity on the surface, it is recognized as magma chamber activity in the deep crust. For the latter two cases, the enhancement of the magnetic anomaly indicates that the magmatic activity was at the same time or earlier than the Martian engine; otherwise, it indicates that the magmatic activity was after the Martian engine stopped.

4. Results

4.1 Results of Morphology and gravity/magnetic inversion

There are several explanations of the cone shapes where Zhurong landed, including mud volcano effects, volcano effects, water volcano effects, etc. (Wu, 2021). We collected 590 cone shapes from the HiRIC image and found that they were of low intensity after we observed their shapes. As shown in Figure 7(a), the craters left on the mud volcanoes by aerolites are larger in diameter. These craters have simpler structures without concentric cycle shapes. According to the experiments by Kawakami, etc. (1983) and Miautani, etc. (1983), we believe these cones are composed of loose mud rock with lower intensity instead of basalt with high intensity (Figure 7(b)). In addition, some cones are found in the form of mud flow (Figure. 7(c)(d)), which also shows that the cones are from mud volcanoes rather than lava volcanoes. Studies from Ivanov, etc. (Ivanov, 2014) show that mud upwelled beneath the Utopia Planita, spewing out from weak spots to form erosion streams and cones

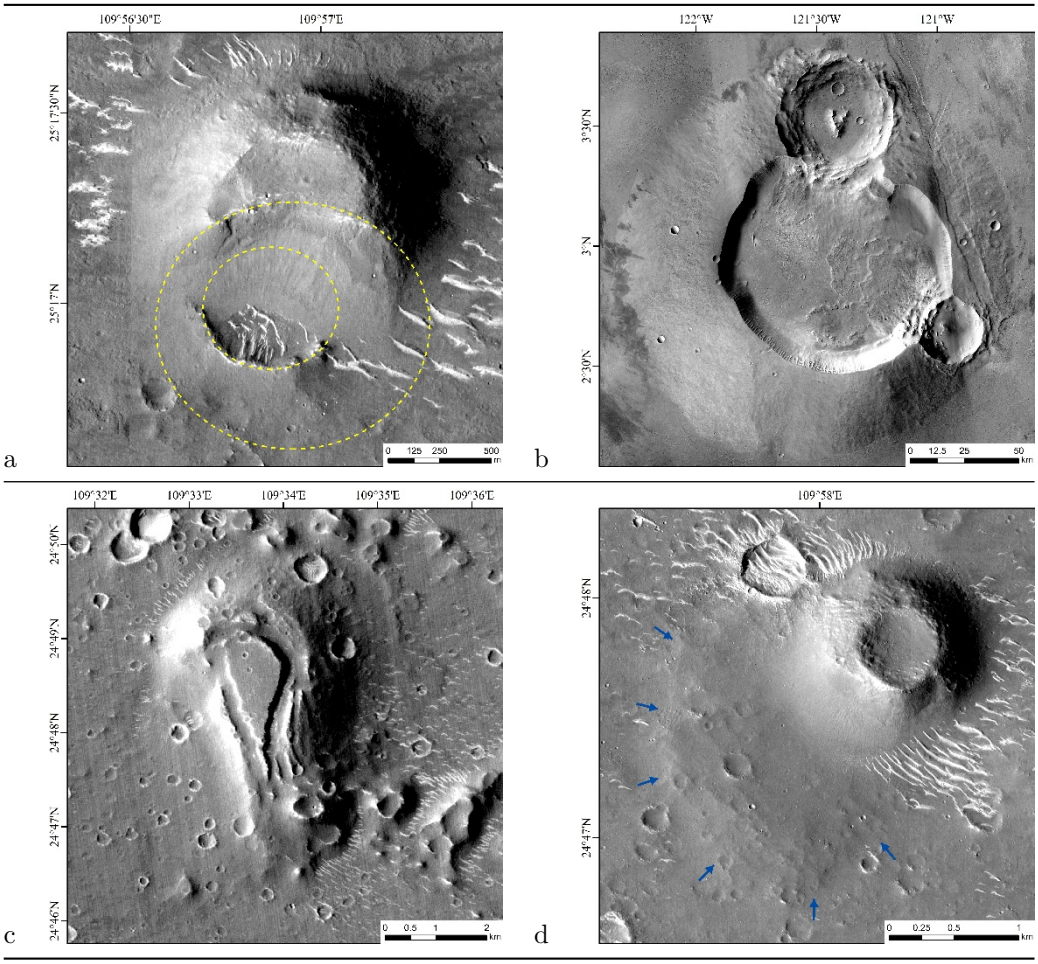

Figure 7. (a) Impacted mud volcano, (b) impacted basalt volcano with concentric circle structure in crater (CTX mosaic ID: E-124_N00), (c) mud volcano with mud flow (CTX mosaic ID: E108_N24), (d) mud volcano with mud flow

The coverage of the ejecta block can be identified by the edge of the steep cliffs with the help of DEM and imaging. The HiRIC image carried by Tianwen-1 can offer a high-resolution DEM to effectively divide ejecta areas. (Figure. 8, as a result mud volcanoes statistics and ejecta division can only be carried out within the coverage of the HiRIC image). On this basis, we calculated the number of mud volcanoes per square kilometer in different areas (Table 2). The results show that mud volcanoes density can reflect ejecta coverage. In areas without ejecta coverage, the number of cones per square kilometer was less than 0.062 (Table 2, blocks a, d, f), and in the area with ejecta coverage, the number was more than 0.064 and even over 0.1 as the amount of ejecta increased (Table 2, blocks c, e, g).

Table 2: Mud volcanoes data statistics in different blocks

Blocks	Type	Mud volcanoes quantity	Area/km^2	Mud volcanoes density/km^{-2}
a	original surface	7	2248.22	0.003114
b	ghost crater ejecta	0	30.11	0
c	ejecta	185	2850.93	0.064903
d	original surface	48	786.85	0.061003
e	ejecta	1	6.03	0.165729
f	original surface	6	97.94	0.061601
g	ejecta	343	2975.82	0.115262

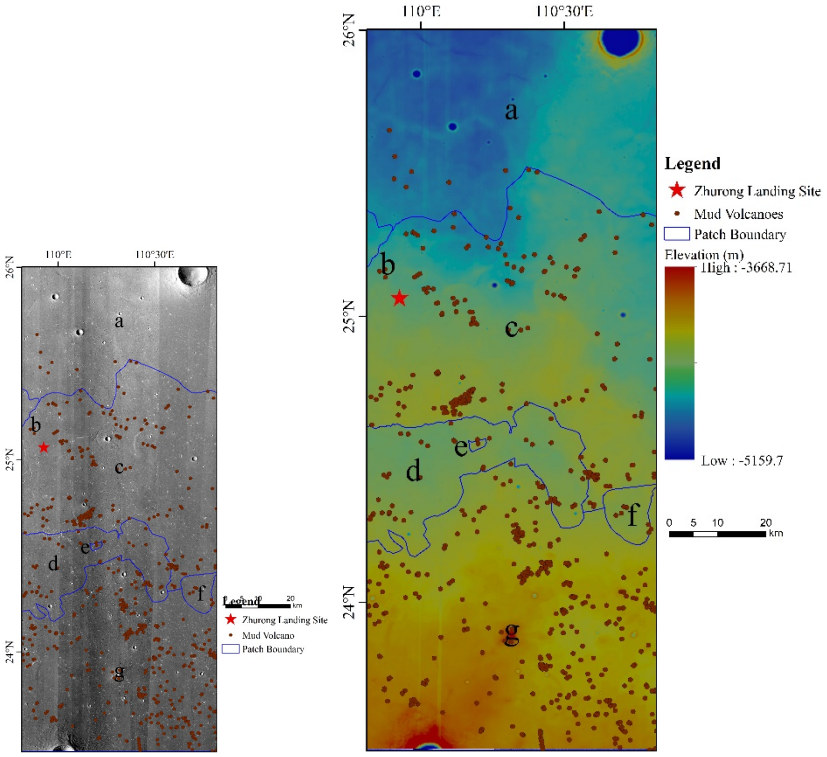

Figure 8. Ejecta blocks division and mud volcanoes distribution map. Base map: HiRIC panchromatic images and DEM, Brown dot: mud volcano, Blue line: Block boundary.

As shown in Figure 9(a), the crustal thickness map shows a red area with thick crust in the southeast, which overlaps with the 50 nT isoline coverage area in the southeast. Many cones and mesas (Figure. 9(b)) can be seen in the CTX image. We infer that deep magmatic activity has resulted in crustal thickening and weak magnetic anomalies. Mittelholz, etc. (2020) believed that the dynamo of 4.5~3.7 Ga activity caused magnetization of the Mars crust. In reference to

his opinion, we think that the weak magnetism in this region formed in the Utopia Planita and was caused by the heating of deep magmatic activity after the Mars dynamo was stopped.

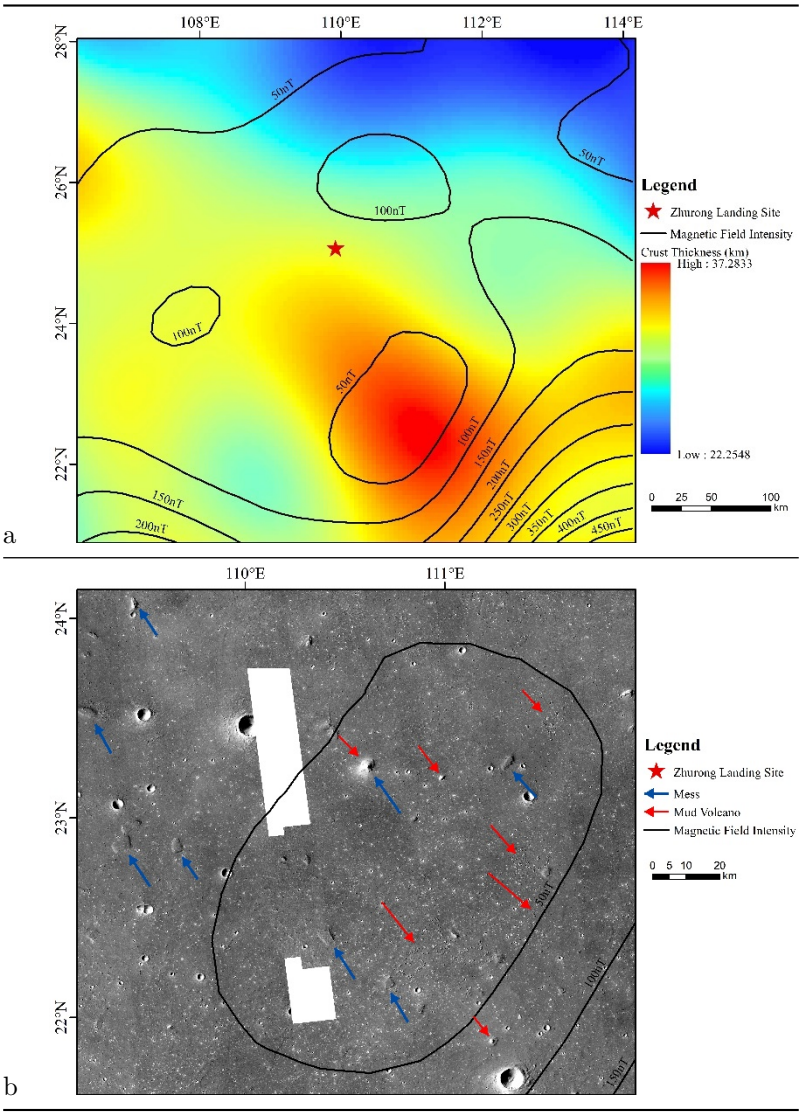

Figure. 9. (a) Crustal thickness and magnetic field intensity of the Zhurong landing site, base map: crustal thickness of the landing site, isoline: magnetic field intensity of the landing site; (b) Geomorphic map of gravity and magnetic anomaly area, blue arrow: mesas; red arrow: mud volcano (CTX mosaic ID: E108_N20, E108_N24).

4.2 CSFD dating results

The existing geological map shows that the Zhurong landing site was formed in the Late Hesperian, which may have experienced a complex evolutionary history such as the Noah impact, volcanic lava filling in the Early Hesperian, and ancient lakes forming and disappearing in the Late Occidental Period (Wu, 2021). In our study, 14,000 craters (with diameters greater than 200 m, Figure 10(b)) were extracted within 200×200 km for dating. The dating results were 1.66 Ga, 3.43 Ga and 3.66 Ga (Figure. 10(b)), which were consistent with earlier studies (Wu, 2021). The dating results show that the VB unit of the Zhurong landing site surface was formed at approximately 3.43 Ga, and the formation of Utopia Planita occurred earlier than 3.66

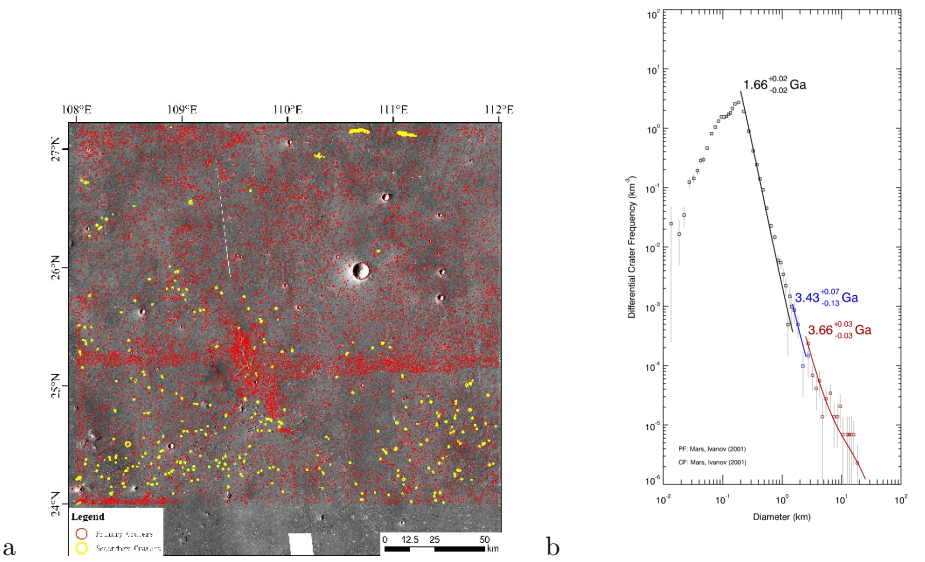

Figure 10. (a) Schematic diagram of crater extraction (CTX mosaic ID: E104_N20, E104_N24, E108_N20, E108_N24, E112_N20, E112_N24), (b) dating image of the Zhurong landing site.

4.3 The 3D strata model

Since flat-bottomed craters reflect the boundary between different strata, we selected 37 flat-bottomed craters within the 2°×2° range around the Zhurong landing site (serious craters have been filled with removed sand, and some deep craters expose two strata) with diameters ranging from 490 m to 8.3 km. The CTX DEM and HiRIC DEM were used to measure the depth of the strata in the

landing site. Figure 11(a) shows the measured depth of the selected flat-bottled crater and the stratum protruding point. The strata identified by craters in the Zhurong landing site are VB in the Late Hesperian. The first stratum is in a dry sedimentary rock segment, and there are 15 craters exposing the first stratum, which are evenly distributed in the landing site. When at depths 250 m, the craters are corrugated outside (Figure. 6(b)), indicating that the second layer has a high water content, which is consistent with the formation background of the VB material. Therefore, we infer that the formation is a humid sedimentary rock segment. The boundary between strata 2 and 3 was measured not only in the smaller flat-bottomed crater but also in the crater wall 68 km northeast of the landing site (red circle in Figure. 11(b)). Seven craters expose the second stratum, most of which are in the western half of the study area. The third stratum is deep and only appears in the bottom center of the crater in Figure 11(b) (also the crater in Figure 6(c)). Because the bottom of the larger crater is often filled, the third stratum cannot be observed. Only the barrier of the large crater indicates that this layer contains plenty of water/ice and belongs to the VB segment. The measured depths of the three strata from the flat-bottomed craters are as follows: the first stratum extends from the surface to a depth of 90-210 m underground, the second extends to a depth of 250-360 m and the third extends to 900 m underground, which is the deepest stratum identified in this experiment. In addition, a large number of cones, similar in shape and size to mud volcanoes on Earth, are present in the area, indicating intense hydrothermal activity in the past. The topographic features also indicate many ejecta scattered over the surface. After measurement, the ejecta has 23 corresponding craters, which are between 15 and 100 meters thick and can cover more than 60 percent of the landing site surface.

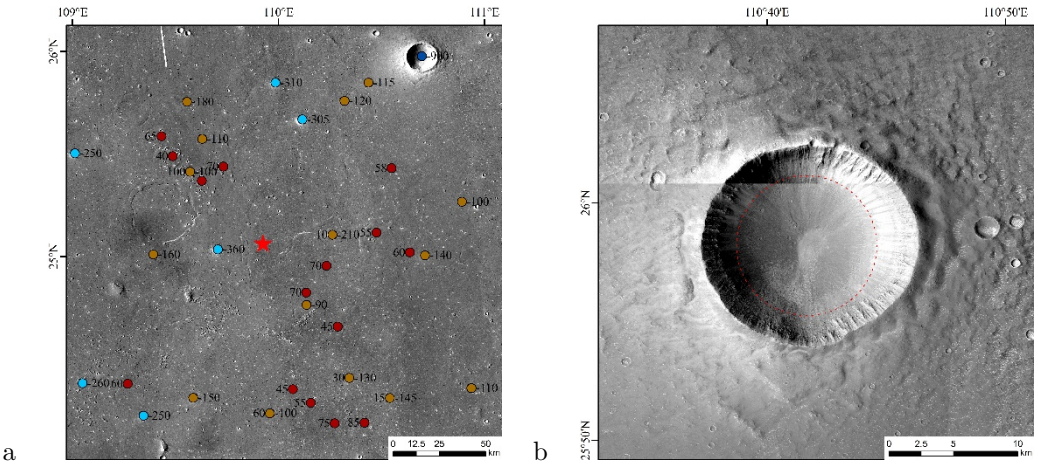

Figure 11. (a) Strata measurement points of the Zhurong landing site, red: ejecta stratum, brown: first stratum, light blue: second stratum, dark blue:

third stratum (CTX mosaic ID: E108_N24); (b) boundary outcrops of strata 2 and 3 on crater walls (base map: CTX mosaic E108_N24, HiRIC panchromatic images).

Based on the formation measurement results obtained, we further developed a 3D formation model (Figure 12). First, the measurement points in the same stratum are selected, and an irregular triangular network (TIN) is made to form the model of the ejecta block and the interface of each stratum. Blocks are then fabricated within the range of adjacent TINs to form a model of stratigraphic structure. According to the material composition of each stratum, the appropriate symbol texture filling blocks are selected, and the three-dimensional stratum model that reflects the stratum burial, depth and thickness, occurrence and rock properties is finally made.

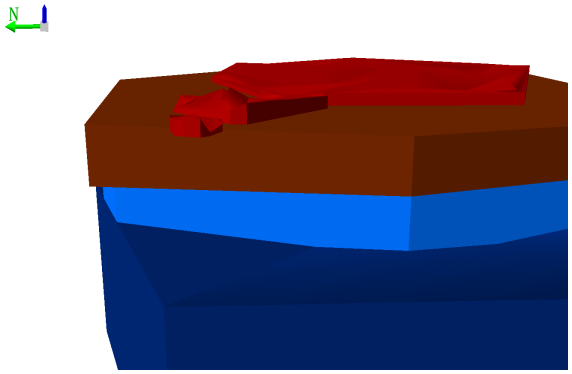

Figure 12. 3D strata model of the Zhurong landing site: red: ejecta block; brown: dry sedimentary rock; light blue: wet sedimentary rock; dark blue: VB.

In the 3D strata model, the brown stratum represents the first stratum, which is a dry sedimentary rock segment located 90-210 m down the surface. The wet light blue stratum represents the second stratum, which is a section of wet sedimentary rock. It is 250-360 m below the dry sedimentary stratum, which had plenty of water interaction in the past. The third stratum is shown in dark blue as the VB segment. All three strata are composed of VB material. In addition, there are patches of ejecta in the first formation (shown in red in the 3D formation model). The 3D strata model shows that the wet sedimentary rock layer gradually thickens from south to north, which is consistent with the trend of VB gradually thickening from periphery to center in the whole Utopia Planita (Buczkowski, 2004), indicating that our 3D strata model can accurately reflect the underground structure.

Analysis

5.1 Structure of the Aquifer

The 3D strata model shows that the VB thickness of the Zhurong's landing site is over 900 m. In addition, we also use the method proposed by Buczkowski et al. (2004) to calculate the VB thickness of the two ghost craters closest to the Zhurong landing site and show that the VB thickness is 1.2 km. Some researchers have also studied the aquifer of the Zhurong landing site. Mills et al. (2021) inferred the VB thickness based on the six ghost craters at the Zhurong landing site, and the average coverage thickness of the four was approximately 1.2 km, which is aligned with our results. The other two ghost craters are approximately 0.6 km thick. However, the results of Wu et al. (2021) show that the VB thickness in this region is 65.5-268.3 m. They believe that VB is greater than the height of the buried crater rim and therefore use the relationship between the edge height of the fresh crater and the diameter of the crater (Garvin, 2003) to estimate the edge height of the ghost crater as the VB thickness. These two vastly different results are due to different interpretations of ghost craters. We believe that it is far from sufficient to estimate the VB thickness by burying the crater edge alone, which would result in the wall of the ghost crater being exposed after volume compaction, which obviously did not occur at the ghost crater in the Zhurong landing site. In addition, when the crater is deeper than 250 m, the content of volatile components reflected in the sputtering mat morphology also gradually increases (Figure 13(A-c)). It is hard to imagine that VBs less thick than 270 m can form barrier craters deeper than 1 km. Finally, a crater 275 km southeast of the landing site, as shown in Figure 13(c), also shows that the VB thickness is much higher than the estimate by Wu et al. (2021). The CTX image shows that part of the impact crater 4800 m below the surface is buried by liquid material similar to mud. Its morphology is markedly different from that of the crater (Figure 13(d)) in the southeastern Utopia Planita, which was filled with lava from the Elysium Volcano. However, there is no source of liquid material on the exposed wall of the crater. The lip of the crater is intact, and there is no indication of significant erosion. Therefore, we judge that the liquid filling material is the VB material pouring from the covered part of the crater.

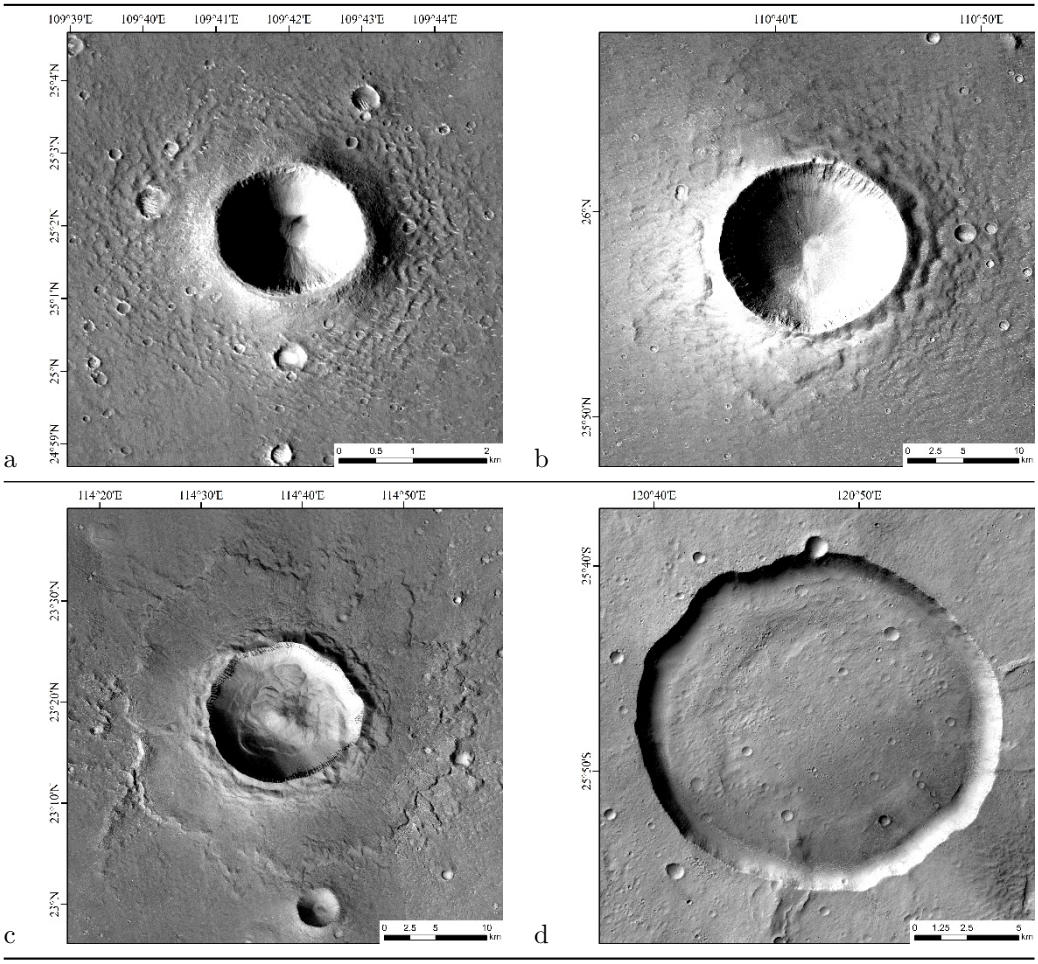

Figure 13. Comparison of sputtering mat morphology and filling morphology of mud and volcanic lava in the craters of various sizes:(a) 1.8 km in diameter, 360 m in depth (CTX mosaic ID: E108_N24); (b) 8 km in diameter, 900 m in depth (CTX mosaic ID: E108_N24); (c) 14 km in diameter and 860 m in depth, filled by upwelling mud (CTX mosaic ID: E112_N20); (d) 17 km in diameter and 400 m in depth, filled with volcanic lava (CTX mosaic ID: E120_N-26).

In summary, we believe that the thickness of the VB group at the Zhurong landing site is 1.2 km. As the Martian climate changed from humid to dry, the difference in the water loss rate of VB at various depths resulted in the consolidation and diagenesis of VB materials in distinct periods and finally formed the three-strata structure in the three-dimensional geological structure.

5.2 Confirmation and genesis of mud volcanoes

Oehler et al. (2010) analyzed the cone of the Acidalia Planita and judged it as a mud volcano. However, Wu et al. (2021) believe that the cone in the landing area of Zhurong does not have similar flow characteristics to mud volcanoes in the Asidalia Plain. After studying the cone in the Hephaestus Fossae area, 823 km southeast of the Zhurong landing site, Dapremont (2021) and others believe that it lacks fluidity, and the near-infrared spectrum at the edge of the vertebral body has the characteristics of olivine, which is considered to be the product of igneous rock. In addition, Soare et al. (2005, 2013, 2020) and Depablo et al. (2009) proposed the possibility of ice core mounds.

In fact, Oehler et al. (2010) pointed out that the morphology of mud volcanoes is diverse, which is also consistent with the conditions at the Zhurong landing site. In addition, from the pictures provided by Wu et al. (2021), it seems that they focus on the clustered cone, ignoring the fluidity phenomenon shown in Figure 7 (cd) of this paper. Due to the lack of cracks in HiRIC images with sufficient resolution, as analyzed by Oehler et al. (2010), these cones are unlikely to be ice core mounds. However, Depablo et al. (2009) still has a high reference value for mud volcanoes because, like ice core mounds, mud volcanoes also need enough heat to melt the buried ice.

Rodriguez et al. (2012) proposed that due to the pressurization of the aquifer, cracks were generated through the overlying cryosphere, and the fluid sediment mixture erupted through the pipeline composed of these cracks to form mud volcanoes. Soare et al. (2005, 2013, 2020) believe that the cone at the Zhurong landing site shows that the area has experienced intense hydrothermal activity. However, there is no obvious magmatic erosion and not sufficiently deep crater in this area to reveal the structure below the VB formation. The spatial statistical, gravity and magnetic results provide clues for confirming the power source of mud volcanoes in this area. The statistical results show that the mud volcano density of the ejecta block at the Zhurong landing site increases significantly from north to south (Figure. 14 (a)), and traces of underground magmatism are revealed by gravity and magnetic observations in the southeastern Zhurong landing site. Combined with the distribution characteristics of mud volcanoes, we judge that the magmatism here provides energy for hydrothermal activities such as mud volcanoes. This also confirms the judgment of Depablo et al. (2009) that there may be a heat source of magma chamber under the surface of Utopian basin (Figure. 14 (b)).

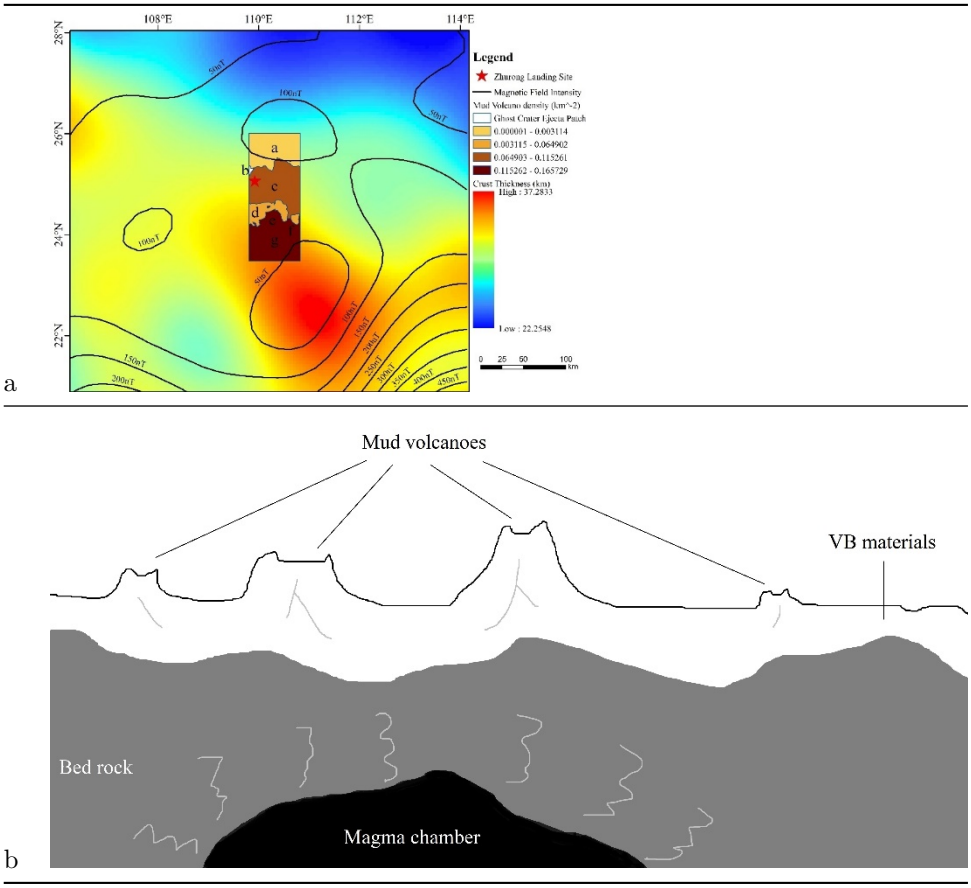

Figure 14 (a) Density distribution, gravity and magnetic anomaly map of mud volcanoes; (b) Mud volcanoes genesis.

5.3 Influence of mud volcanism on ghost craters

There is a 19 km diameter ghost crater 30 km west of the Zhurong landing site. Such ghost craters are widely distributed in the southern Utopian Planita. At present, its genesis includes differential compaction folds (Mcgill and Hills, 1992), the second graben formed by fold horizontal extension (Hobbs, 1967) and volumetric compaction (Buczkowski, 2004). Among them, the viewpoint of volume compaction considers the process of downward compaction of overburden materials along the inclined pit wall, which accurately explains the double ring graben of ghost crater. However, the inner graben of the ghost crater on the west side of the Zhurong landing site (Figure. 15 (a)) is much deeper than the outer graben, and the elevation within the inner graben is also significantly lower than that outside (approximately 80 m), showing stronger compaction. However, some ghost craters do not have such a significant internal and external elevation

difference (Figure. 15 (b)). Therefore, the shape of the ghost crater on the west side of Zhurong may be dominated by more than the compaction caused by water evaporation. In cases where there are a vast number of mud volcanoes and ejecta blocks covering ghost craters, we calculated that the material loss of ghost craters was around 12.504 km^3 by utilizing the MEX HRSC MOLA blended DEM and 3D strata model. The volumes of the two muddy ejecta blocks are 1.244 km3×10.940 km^3. The sum of them is close to the mass loss due to the ghost impacting force. This indicates that at places with drastic water thermal activity, such as Zhurong landing, in the process of forming ghost craters after the crater is buried by the VB, the upwelling and ejection of underground materials also plays a role in controlling the morphology of ghost craters.

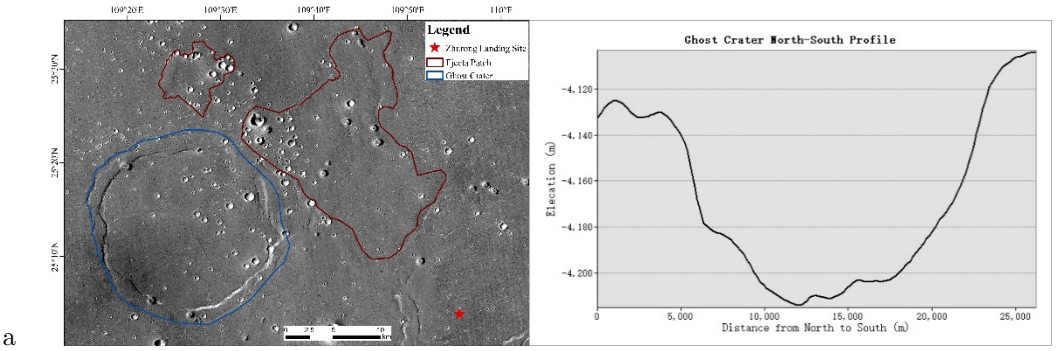

Figure 15 (a) Ghost crater and topographic profile west of the landing site, blue: Ghost crater, red: ejecta block (CTX mosaic ID: E108_N24); (b) Ghost crater without material loss and its topographic profile (CTX mosaic ID: E104_N24, E108_N24).

Conclusion

We have derived more than 14000 craters at the Zhurong landing site and conducted geological dating. By taking advantage of the CTX image, we produced a DEM of the Zhurong landing site. By

measuring 37 exposured strata due to craters on the CTX DEC and HiRIC DEM and combining the morphological features of craters and the structural background of the site, we produced a 3D strata model for the Zhurong landing site. Utilizing heavy magnetic data and morphological features, we have determined that the widely distributed cones on the Zhurong landing site are mud volcanoes, and we further divide them into the distribution range of muddy ejecta blocks based on their distribution characteristics and surface landforms. Combining the 3D strata model and ejecta block distribution, we discussed the motion mechanism in the formation process of ghost craters.

The major conclusions are as follows:

1. The Zhurong landing site can be divided into 3 strata and ejecta blocks. The strata of the Zhurong landing site can be defined as dry sediment members, moist sediment members and VB members from the top to the bottom. The width of VB group can amount to 1.2 km.

2) The morphological features show that the cones at the Zhurong landing site are mud volcanoes formed by underground water thermal activity. The heat source comes from the magma chamber located in the southern underground part. The density of the mud volcanoes can help determine whether the ejecta block exists.

3) The 3D strata model of the Zhurong landing site indicates that apart from volume compaction, some ghost craters have underground material ejection, resulting in the internal elevation being significantly lower than the external elevation

4 Currently, the Zhurong Rover is moving north; if it can arrive at the heavy magnetic abnormal area, the in situ detection data obtained are expected to provide more clues for possible underground magmatism and its transformation to the surface in this area. We look forward to more data returned by Zhurong Rover and Tianwen-1 in the future to further enrich the research on the geological evolution history of the landing inspection area.

7. Acknowledgements and Data

This work was supported by National Key Research and Development project (2019YFE0123300), Civil Aerospace Technology Pre-research Project of National Defense Science and Industry Administration (No.D020103); Beijing Science and Technology Project (No.Z191100004319001).

The Tianwen-1 data used in this work is processed and produced by the Ground Research and Application System (GRAS) of China's Lunar and Planetary Exploration Program, provided by China National Space Administration (http://moon.bao.ac.cn). The HiRIC DEM and HiRIC panchromatic images titles are listed in the following table, these data's acquisition are within

protection period now, an account is needed to apply for them. But some of them can directly achieved at https://moon.bao.ac.cn/web/enmanager/zygj without account and application. The CTX mosaic images produced by the Malin Space Science Systems and Jet Propulsion Laboratory and panchromatic images are available at http://murray-lab.caltech.edu/CTX/tiles/beta01_tile-blended/. The MEX HRSC MOLA blended DEM is publicly available at https://astrogeology.usgs.gov/search/map/Mars/Topography/HRSC_MOLA_Blend/Mars_HRSC_MOLA_ Crustal thickness data can be obtained from NASA's Planetary Data System (PDS): https://ode.rsl.wustl.edu/mars/indexDatasets.aspx.

Table: HiRIC DEM and panchromatic images titles

Titles	Directly achieved (T/F)
HX1_GRAS_HIRIC_DEM_3.5_0000_244453N1101905E_A	T (equal to MosaicDEM_3.5.tif)
HX1_GRAS_HIRIC_DIM_0.7_0001_254537N1095850E_A	F
HX1_GRAS_HIRIC_DIM_0.7_0002_254537N1101905E_A	F
HX1_GRAS_HIRIC_DIM_0.7_0003_254537N1103919E_A	F
HX1_GRAS_HIRIC_DIM_0.7_0004_251515N1095850E_A	T
HX1_GRAS_HIRIC_DIM_0.7_0005_251515N1101905E_A	F
HX1_GRAS_HIRIC_DIM_0.7_0006_251515N1103919E_A	F
HX1_GRAS_HIRIC_DIM_0.7_0007_244453N1095850E_A	T
HX1_GRAS_HIRIC_DIM_0.7_0008_244453N1101905E_A	F
HX1_GRAS_HIRIC_DIM_0.7_0009_244453N1103919E_A	F
HX1_GRAS_HIRIC_DIM_0.7_0010_241431N1095850E_A	F
HX1_GRAS_HIRIC_DIM_0.7_0011_241431N1101905E_A	F
HX1_GRAS_HIRIC_DIM_0.7_0012_241431N1095850E_A	F
HX1_GRAS_HIRIC_DIM_0.7_0013_234409N1095850E_A	F
HX1_GRAS_HIRIC_DIM_0.7_0014_234409N1101905E_A	F
HX1_GRAS_HIRIC_DIM_0.7_0015_234409N1103919E_A	F

Reference

1. Wan, W.X., Wang, C., Li, C.L. et al. China's first mission to Mars. Nat Astron 4, 721 (2020). https://doi.org/10.1038/s41550-020-1148-6

2. Depablo, M., & Komatsu, G. (2009). Possible pingo fields in the Utopia basin, Mars: Geological and climatical implications. Icarus, 199(1), 49-74. doi:10.1016/j.icarus.2008.09.007

3. Soare, R. J., Burr, D. M., & Wan Bun Tseung, J. M. (2005). Possible pingos and a periglacial landscape in northwest Utopia Planitia. Icarus, 174(2), 373-382. doi:10.1016/j.icarus.2004.11.013

4. Soare, R. J., Conway, S. J., Pearce, G. D., Dohm, J. M., & Grindrod, P. M. (2013). Possible crater-based pingos, paleolakes and periglacial landscapes at the high latitudes of Utopia Planitia, Mars. Icarus, 225(2), 971-981. doi:10.1016/j.icarus.2012.08.041

5. Soare, R. J., Conway, S. J., Williams, J. P., Gallagher, C., & Keown, L. E. M. (2020). Possible (closed system) pingo and ice-wedge/thermokarst complexes at the mid latitudes of Utopia Planitia, Mars. Icarus, 342. doi:10.1016/j.icarus.2019.03.010

6. Ivanov, M. A., Hiesinger, H., Erkeling, G., & Reiss, D. (2014). Mud volcanism and morphology of impact craters in Utopia Planitia on Mars: Evidence for the ancient ocean. Icarus, 228, 121-140. doi:10.1016/j.icarus.2013.09.018

7. Mangold, N., Gupta, S., Gasnault, O., Dromart, G., Tarnas, J. D., Sholes, S. F., . . . Williford, K. H. Perseverance rover reveals an ancient delta-lake system and flood deposits at Jezero crater, Mars. Science, 0(0), eabl4051. doi:doi:10.1126/science.abl4051

8. Wu, X., Liu, Y., Zhang, C., Wu, Y., Zhang, F., Du, J., . . . Zou, Y. (2021). Geological characteristics of China's Tianwen-1 landing site at Utopia Planitia, Mars. Icarus, 370. doi:10.1016/j.icarus.2021.114657

9. Long Xiao, Peimin Zhu, Guangyou Fang, Zhiyong Xiao, Yongliao Zou, Jiannan Zhao, Na Zhao, Yuefeng Yuan, Le Qiao, Xiaoping Zhang, Hao Zhang, Jiang Wang, Jun Huang, Qian Huang, Qi He, Bin Zhou, Yicai Ji, Qunying Zhang, Shaoxiang Shen, Yuxi Li, Yunze Gao. A young multilayered terrane of the northern Mare Imbrium revealed by Chang'E-3 mission [J]. Science, 2015,347(6227).

10. Yuan Y, Zhu P, Zhao N, et al. The 3-D geological model around Chang 'E-3 landing site based on lunar penetrating radar Channel 1 data[J]. Geophysical Research Letters, 2017, 44(13).

11. Yue, Z., Di, K., Liu, Z., Michael, G., Jia, M., Xin, X., . . . Liu, J. (2019). Lunar regolith thickness deduced from concentric craters in the CE-5 landing area. Icarus, 329, 46-54. doi:10.1016/j.icarus.2019.03.032

12. McGill, G. E. (1989), Buried topography of Utopia, Mars: Persistence of a giant impact depression,Journal of Geophysical Research: Solid Earth (1978–2012),94(B3), 2753–2759.

13. Thomson, B. J., and Head, J. W. (2001), Utopia Basin, Mars: Characterization of topography and morphology and assessment of the origin and evolution of basin internal structure, J. Geophys. Res., 106(E10), 23209–23230, doi:10.1029/2000JE001355..

14. Masursky, H., & Crabill, N. L. (1976). Search for the Viking 2 landing site. Science, 194(4260), 62-68.

15. Mills, M. M., McEwen, A. S., & Okubo, C. H. (2021). A Preliminary Regional Geomorphologic Map in Utopia Planitia of the Tianwen-1 Zhurong Landing Region. Geophysical Research Letters, 48(18). doi:10.1029/2021gl094629

16. Tanaka, K. L., & Scott, D. H. (1987). Geologic map of the polar regions of Mars: US Geological Survey Miscellaneous Investigations Series. Map I-1802-C, scale: 1: 2,000,000.

17. Kreslavsky, M. A., and Head, J. W., Mars: Nature and evolution of young latitude-dependent water-ice-rich mantle, Geophys. Res. Lett., 29(15), doi:10.1029/2002GL015392, 2002.

18. Goossens, S., Sabaka, T. J., Genova, A., Mazarico, E., Nicholas, J. B., & Neumann, G. A. (2017). Evidence for a Low Bulk Crustal Density for Mars from Gravity and Topography. Geophys Res Lett, 44(15), 7686-7694. doi:10.1002/2017GL074172

19. Langlais, B., Thébault, E., Houliez, A., Purucker, M. E., & Lillis, R. J. (2019). A new model of the crustal magnetic field of Mars using MGS and MAVEN. Journal of Geophysical Research: Planets, 124, 1542– 1569. https://doi.org/10.1029/2018JE005854

20. Dickson, J. L., Kerber, L. A., Fassett, C. I., & Ehlmann, B. L. (2018, March). A global, blended CTX mosaic of Mars with vectorized seam mapping: A new mosaicking pipeline using principles of non-destructive image editing. In Lunar and planetary science conference (Vol. 49, pp. 1-2).

21. Meng, Q., Wang, D., Wang, X., Li, W., Yang, X., Yan, D., . . . Dong, J. (2021). High Resolution Imaging Camera (HiRIC) on China's First Mars Exploration Tianwen-1 Mission. Space Science Reviews, 217(3), 42. doi:10.1007/s11214-021-00823-w

22. McEwen, A. S., Eliason, E. M., Bergstrom, J. W., Bridges, N. T., Hansen, C. J., Delamere, W. A., . . . Weitz, C. M. (2007). Mars Reconnaissance Orbiter's High Resolution Imaging Science Experiment (HiRISE). Journal of Geophysical Research, 112(E5). doi:10.1029/2005je002605

23. Malin, M. C., Bell, J. F., Cantor, B. A., Caplinger, M. A., Calvin, W. M., Clancy, R. T., . . . Wolff, M. J. (2007). Context Camera Investigation on board the Mars Reconnaissance Orbiter. Journal of Geophysical Research, 112(E5). doi:10.1029/2006je002808

24. Fergason, R. L, Hare, T. M., & Laura, J. (2018). HRSC and MOLA Blended Digital Elevation Model at 200m v2. Astrogeology PDS Annex, U.S. Geological Survey. http://bit.ly/HRSC_MOLA_Blend_v0

25. Barlow, N. G. (2006). Impact craters in the northern hemisphere of Mars: Layered ejecta and central pit characteristics. Meteoritics & Planetary Science, 41(10), 1425-1436. doi:https://doi.org/10.1111/j.1945-5100.2006.tb00427.x

26. Niu, S., Zhang, F., Di, K., Gou, S., & Bugiolacchi, R. (2021). Dating and Morphological Characterization of Layered Ejecta Craters in the

Candidate Landing Areas of China's First Mars Mission (Tianwen-1). https://ui.adsabs.harvard.edu/abs/2021LPI....52.1786N

27. Dapremont, A. M., & Wray, J. J. (2021). Igneous or Mud Volcanism on Mars? The Case Study of Hephaestus Fossae. Journal of Geophysical Research: Planets, 126(2). doi:10.1029/2020je006390

28. Wilcox, B. B., Robinson, M. S., Thomas, P. C., & Hawke, B. R. (2005). Constraints on the depth and variability of the lunar regolith. Meteoritics & Planetary Science, 40(5), 695-710. doi:DOI 10.1111/j.1945-5100.2005.tb00974.x

29. Wieczorek, M. A., and Zuber, M. T. (2004), Thickness of the Martian crust: Improved constraints from geoid-to-topography ratios, J. Geophys. Res., 109, E01009, doi:10.1029/2003JE002153.

30. Mittelholz, A., Johnson, C. L., Feinberg, J. M., Langlais, B., & Phillips, R. J. (2020). Timing of the martian dynamo: New constraints for a core field 4.5 and 3.7 Ga ago. Science Advances, 6(18), eaba0513. doi:doi:10.1126/sciadv.aba0513

31. Gong, S., & Wieczorek, M. (2021). Depth of Martian Magnetization From Localized Power Spectrum Analysis. Journal of Geophysical Research: Planets, 126(8). doi:10.1029/2020je006690

32. Kawakami, S.-I., Mizutani, H., Takagi, Y., Kato, M., & Kumazawa, M. (1983). Impact experiments on ice. Journal of Geophysical Research: Solid Earth, 88(B7), 5806-5814. doi:10.1029/JB088iB07p05806

33. Mizutani, H., Kawakami, S.-i., Takagi, Y., Kato, M., & Kumazawa, M. (1983). Cratering experiments in sands and a trial for general scaling law. Journal of Geophysical Research, 88(S02). doi:10.1029/JB088iS02p0A835

34. Buczkowski, D. L., and Cooke, M. L. (2004), Formation of double-ring circular grabens due to volumetric compaction over buried impact craters: Implications for thickness and nature of cover material in Utopia Planitia, Mars, J. Geophys. Res., 109, E02006, doi:10.1029/2003JE002144.

35. McGill, G. E., and L. S. Hills (1992), Origin of giant Martian polygons, J. Geophys. Res., 97, 2633–2647.

36. Hobbs, D. W. (1967), The formation of tension joints in sedimentary rocks: An explanation, Geol. Mag., 104, 550–556.

37. Garvin, J. B., Sakimoto, S. E. H., & Frawley, J. J. (2003, July 01, 2003). Craters on Mars: Global Geometric Properties from Gridded MOLA Topography.

38. Oehler, D. Z., & Allen, C. C. (2010). Evidence for pervasive mud volcanism in Acidalia Planitia, Mars. Icarus, 208(2), 636-657. doi:10.1016/j.icarus.2010.03.031